



CrossMark
click for updates

Cite this: *Chem. Sci.*, 2015, 6, 3003

Ru(II)–Re(I) binuclear photocatalysts connected by –CH₂XCH₂– (X = O, S, CH₂) for CO₂ reduction†

Eishiro Kato,^a Hiroyuki Takeda,^{ab} Kazuhide Koike,^{bc} Kei Ohkubo^a and Osamu Ishitani^{*ab}

We developed Ru(II)–Re(I) supramolecular photocatalysts in which each metal complex unit is connected by a –CH₂XCH₂– (X = O, S, CH₂) chain. The photocatalyst with X = O exhibited the best photocatalytic efficiency for CO₂ reduction in the reported systems using a NAD(P)H model compound as an electron donor because the introduced oxygen atom strengthened the oxidation power of the Ru photosensitizer unit in the excited state and accelerated electron transfer from the one-electron-reduced Ru photosensitizer unit to the Re catalyst unit. In contrast, the catalytic ability of the photocatalyst with X = S rapidly decreased during irradiation because the supramolecular structure split into mononuclear complexes. A detailed mechanism for the efficient photocatalytic reaction involving these supramolecular photocatalysts was investigated for the first time.

Received 1st December 2014
Accepted 28th February 2015

DOI: 10.1039/c4sc03710c

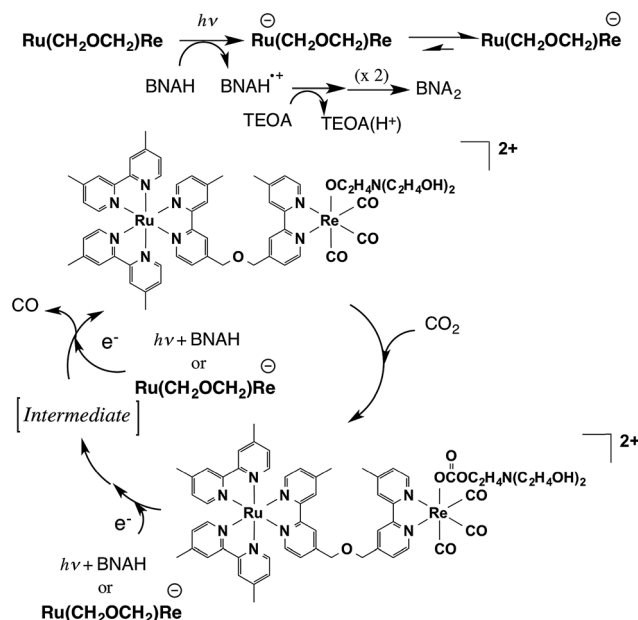
www.rsc.org/chemicalscience

Introduction

The conversion of CO₂ into high-energy compounds using solar energy is a potential technology for addressing both the problem of global warming and the shortage of fossil fuel resources.¹ Some transition metal complexes can broadly absorb visible light and function as redox photosensitizers, which drive one-electron-transfer reactions.² However, because the reduction of CO₂ to stable compounds requires multi-electron insertion into CO₂, a catalyst is also required for photocatalytic CO₂ reduction systems.³ Electrochemical catalysts for CO₂ reduction using transition metal complexes⁵ or a pyridinium cation⁶ have been developed, and some of them have been applied for photocatalytic systems with redox photosensitizers.⁷ As typical examples, mixed systems consisting of [Ru(N[^]N)₃]²⁺ (N[^]N = diimine ligand) as a photosensitizer and

Co, Ni, and Ru complexes as a catalyst have been reported to photocatalyze CO₂ reduction to CO and/or HCOOH using visible light.⁴

We have developed supramolecular photocatalysts with a Ru(II) photosensitizer and a Re(I) catalyst connected to each other *via* a bridging ligand consisting of two diimine moieties connected with an alkyl chain,⁸ *e.g.*, Ru(CH₂CH₂)Re (Chart 1); the quantum yield (Φ_{CO}) and the turnover number (TON_{CO}) of



Scheme 1 Partial reaction mechanism of photocatalytic CO₂ reduction by Ru(CH₂OCH₂)Re.

^aDepartment of Chemistry, Graduate School of Science and Engineering, Tokyo Institute of Technology, 2-12-1-NE1, O-okayama, Meguro-ku, Tokyo, 152-8550, Japan. E-mail: ishitan@chem.titech.ac.jp

^bCREST, Japan Science and Technology Agency, 4-1-8 Honcho, Kawaguchi-shi, Saitama 322-0012, Japan

^cNational Institute of Advanced Industrial Science and Technology, 16-1 Onogawa, Tsukuba, Ibaraki 305-8569, Japan

† Electronic supplementary information (ESI) available: Stern–Volmer plots of the dyad; UV-vis spectra of the OERs of Ru and Re; UV-vis spectral changes during the photocatalytic reaction; ESI-MS spectrum of the SEC peak at 36.1 min after the 120 min photocatalytic reaction using Ru(CH₂OCH₂)Re; IR spectral change by the formation of Ru(CH₂OCH₂)Re(CO)₃(X) (X = ⁻OC₂H₄N(C₂H₄OH)₂ or ⁻OC(O)OC₂H₄N(C₂H₄OH)₂); Stern–Volmer plots for Ru(CH₂OCH₂)Re(CO)₃(X) (X = ⁻OC(O)OC₂H₄N(C₂H₄OH)₂); changes of SEC chromatograms, ESI-MS spectra, and IR spectra during the photocatalytic reaction using Ru(CH₂CH₂)Re; changes of a ESI-MS spectrum after the photocatalytic reaction; ESI-MS spectra of the SEC peak at 36.5 min and 37.8 min after the 120 min photocatalytic reaction using Ru(CH₂SCH₂)Re. See DOI: 10.1039/c4sc03710c



CO formation were 0.15 and 207, respectively, by using 1-benzyl-1,4-dihydronicotinamide (BNAH) as a reductant,^{8c} which has been the most efficient supramolecular photocatalyst for CO₂ reduction of those reported.^{8b} The efficiency and durability of these diad photocatalysts are much higher than those of the corresponding mixed systems. However, these systems still have a problem; the low oxidation power of the excited Ru unit of the diads severely limits the kinds of reductants that can be used. For example, only 62% of the excited Ru units of **Ru(CH₂CH₂)Re** were reductively quenched by a relatively high concentration (0.1 M) of BNAH, which has been often used as a sacrificial electron donor. This result means that 38% of the absorbed photons are wasted in the first process of the photocatalytic reaction and cannot be used for CO₂ reduction. Therefore, improvement of the oxidation power of the excited Ru unit is required to enhance the photocatalytic activity of the diad. One method for improving the oxidation ability of the excited Ru unit has been reported: introducing electron-withdrawing groups, *e.g.*, -CF₃, into the peripheral ligands.^{8a} Although greater efficiency of the quench by a reductant could be achieved, the photocatalytic ability of the diad with such a Ru unit for CO₂ reduction was much lower than that of the corresponding diad without the electron-withdrawing groups in the Ru unit. Electron transfer from the reduced Ru unit to the Re unit could not efficiently proceed because the added electron was localized in the peripheral ligands with the electron-withdrawing groups and the redox potential of the Ru unit became more positive than that of the Re unit. Improving the photocatalytic activity of the supramolecular photocatalyst therefore requires both strengthening the oxidation power of the photosensitizer unit and achieving efficient electron transfer from the reduced photosensitizer unit to the catalyst unit.

Recently, we also reported a new hybrid CO₂ reduction photocatalyst in which a supramolecular photocatalyst with phosphate anchor groups was adsorbed onto the semiconductor photocatalyst TaON.⁹ This hybrid photocatalyst exhibited both strong oxidation power and selective reduction power for CO₂ reduction because of the Z-scheme mechanism, in which stepwise two-photon excitation can make both a hole as a powerful oxidant in the valence band of TaON and an electron in the photosensitizer unit of the diad. One of the most important keys to improving the efficiency of this promising hybrid photocatalyst is the reconciliation of the stronger oxidation power of the excited photosensitizer unit and the efficient intramolecular electron transfer in the diad because efficient interfacial electron transfer should proceed from the conduction band of TaON to the excited photosensitizer unit of the diad and then to the catalyst unit during the photocatalytic reduction of CO₂.

In this report, new Ru(II)-Re(I) diads with bridging ligands constructed of two diimines connected by -CH₂OCH₂- or -CH₂SCH₂- were synthesized and investigated as photocatalysts with enhanced oxidation power; their enhanced oxidation power stems from the greater electronegativity of the bridging ligands' oxygen and sulfur atoms compared to that of the central carbon atom in the alkyl chains such as -CH₂CH₂CH₂- (Chart 1). The diad with the -CH₂OCH₂- chain exhibited the best performance

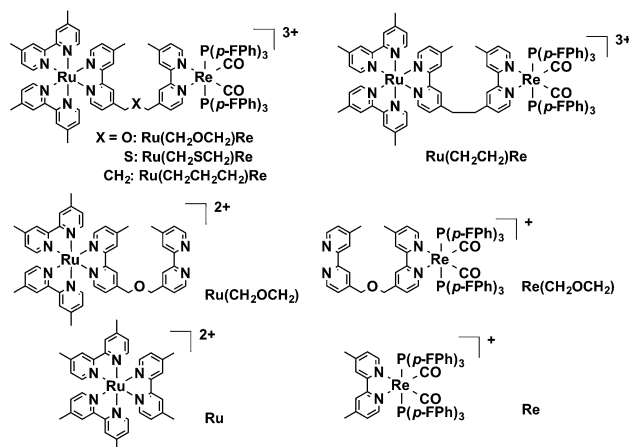


Chart 1 Structures and abbreviations of the metal complexes.

as a supramolecular catalyst for CO₂ reduction using BNAH as the reductant. A detailed mechanism of CO₂ reduction using the Ru-Re diads is also reported for the first time.

Results and discussion

The diads were synthesized by the following method: the reaction of [(dmb)₂RuCl₂]²⁺ (dmb = 4,4'-dimethyl-2,2'-bipyridine) and the bridging ligand gave **Ru(CH₂XCH₂)** (X = O, S, CH₂) with a bridging ligand with a non-coordinated diimine moiety; **Ru(CH₂XCH₂)** was subsequently reacted with [Re(CO)₃{P(*p*-FPh)₃}₂(OTf)] to give **Ru(CH₂XCH₂)Re** in 8–32% yield calculated on the basis of the amount of [(dmb)₂RuCl₂]²⁺ used.

Fig. 1a shows the UV-vis absorption spectra of **Ru(CH₂OCH₂)Re** and its model mononuclear complexes (**Ru(CH₂OCH₂)** and **Re(CH₂OCH₂)**), and Fig. 1b shows those of **Ru(CH₂CH₂CH₂)Re** and its models (**Ru** and **Re**). The spectra of both diads are approximately consistent with the summation spectra of their model complexes, as shown by the dotted lines in the figures. The results indicate that no strong electronic interaction occurs between the Ru and Re units in the ground states of both diads. The broad absorption at 400–550 nm is assignable to metal-to-

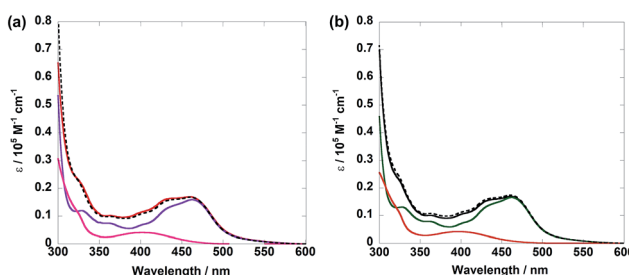


Fig. 1 UV-vis absorption spectra of (a) **Ru(CH₂OCH₂)Re** (red), **Ru(CH₂OCH₂)** (purple), and **Re(CH₂OCH₂)** (pink), and (b) **Ru(CH₂CH₂CH₂)Re** (black), **Ru** (green), and **Re** (red). The dotted lines show the 1:1 summation spectrum of (a) **Ru(CH₂OCH₂)** and **Re(CH₂OCH₂)** and (b) **Ru** and **Re**. Dimethylformamide (DMF) was used as the solvent.



ligand charge-transfer ($^1\text{MLCT}$) absorption of the Ru unit, whereas that at 350–460 nm is attributable to $^1\text{MLCT}$ absorption of both Ru and Re units. The strong absorption band at approximately 300 nm is attributed to $\pi\text{-}\pi^*$ absorption of the diimine ligands of both the Ru and the Re units.

As a typical example of a photocatalytic reaction, a DMF–triethanolamine (TEOA) (5 : 1, v/v) solution containing $\text{Ru}(\text{CH}_2\text{OCH}_2)\text{Re}$ (0.05 mM) and BNAH (0.1 M) as the reductant was irradiated under a CO_2 atmosphere at wavelengths greater than 500 nm; these wavelengths could be absorbed only by the Ru unit. Carbon monoxide was selectively produced along with very small amounts of H_2 and HCOOH (Fig. 2a). The turnover number of CO formation (TON_{CO}) was as high as 253 for 20 h of irradiation. The quantum yield of CO formation (Φ_{CO}) was 0.18, which was determined using monochromic light at $\lambda = 480$ nm (light intensity: 4.3×10^{-9} einstein s^{-1}). Notably, this Φ_{CO} achieved with $\text{Ru}(\text{CH}_2\text{OCH}_2)\text{Re}$ is the highest value among the reported photocatalytic systems in which BNAH was used as the reductant. The other diads also gave CO selectively; the CO formation achieved using each diad is compared in Fig. 2b. The photocatalytic activity of $\text{Ru}(\text{CH}_2\text{OCH}_2)\text{Re}$ ($\Phi_{\text{CO}} = 0.18$, $\text{TON}_{\text{CO}} = 253$) was greater than that of $\text{Ru}(\text{CH}_2\text{SCH}_2)\text{Re}$ ($\Phi_{\text{CO}} = 0.10$, $\text{TON}_{\text{CO}} = 178$); however, both the efficiency and stability of $\text{Ru}(\text{CH}_2\text{SCH}_2)\text{Re}$ ($\Phi_{\text{CO}} = 0.09$, $\text{TON}_{\text{CO}} = 73$) were lower than those of $\text{Ru}(\text{CH}_2\text{CH}_2\text{CH}_2)\text{Re}$.

Fig. 3 shows the emission spectra of the diads. In all cases, broad emission from the $^3\text{MLCT}$ excited state of the Ru unit was observed. The emission maxima of both $\text{Ru}(\text{CH}_2\text{OCH}_2)\text{Re}$ and $\text{Ru}(\text{CH}_2\text{SCH}_2)\text{Re}$ were red-shifted by 10 nm compared to that of $\text{Ru}(\text{CH}_2\text{CH}_2\text{CH}_2)\text{Re}$. The emission quantum yields (Φ_{em}) and emission lifetimes (τ_{em}) of $\text{Ru}(\text{CH}_2\text{OCH}_2)\text{Re}$ and $\text{Ru}(\text{CH}_2\text{SCH}_2)\text{Re}$ decreased compared to those of $\text{Ru}(\text{CH}_2\text{CH}_2\text{CH}_2)\text{Re}$ according to the energy-gap law (Table 1). These emission properties of the Ru units in both $\text{Ru}(\text{CH}_2\text{OCH}_2)\text{Re}$ and $\text{Ru}(\text{CH}_2\text{CH}_2\text{CH}_2)\text{Re}$ were very similar to those of their model mononuclear complexes, *i.e.*, $\text{Ru}(\text{CH}_2\text{OCH}_2)$ and Ru , respectively (Table 1). These similarities strongly suggest that the difference between the emission properties of $\text{Ru}(\text{CH}_2\text{OCH}_2)\text{Re}$ and $\text{Ru}(\text{CH}_2\text{CH}_2\text{CH}_2)\text{Re}$ was mainly caused by the introduction of the oxygen atom into the bridging

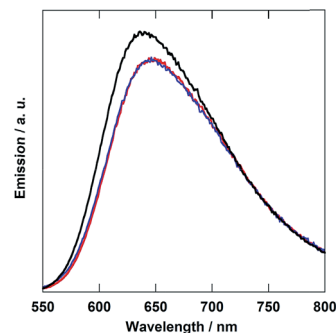


Fig. 3 The emission spectra of $\text{Ru}(\text{CH}_2\text{OCH}_2)\text{Re}$ (red), $\text{Ru}(\text{CH}_2\text{SCH}_2)\text{Re}$ (blue), and $\text{Ru}(\text{CH}_2\text{CH}_2\text{CH}_2)\text{Re}$ (black) collected at 25 °C in DMF; the spectra are normalized to the absorbance of the solutions at $\lambda_{\text{excitation}} = 456$ nm.

ligand; thus, introduction of the Re unit into the opposite side did not strongly affect the emission properties in either case. This result also suggests that intramolecular quenching of the $^3\text{MLCT}$ of the Ru unit by electron and/or energy transfer to the Re unit did not proceed or proceeded with very low efficiency.

Emission from the Ru units in all of the diads was reductively quenched by BNAH, and the Stern–Volmer plots of the emission quenching exhibited good linearity (Fig. S1, ESI†). Table 1 summarizes the quenching rate constants of the emission from the Ru units (k_q) and the quenching fractions with 0.1 M BNAH (η_q). Under the photocatalytic reaction conditions, the η_q values of $\text{Ru}(\text{CH}_2\text{OCH}_2)\text{Re}$ and $\text{Ru}(\text{CH}_2\text{SCH}_2)\text{Re}$ were approximately 10% higher than that of $\text{Ru}(\text{CH}_2\text{CH}_2\text{CH}_2)\text{Re}$. This result strongly suggests that the oxidizing powers of the excited Ru units in $\text{Ru}(\text{CH}_2\text{OCH}_2)\text{Re}$ and $\text{Ru}(\text{CH}_2\text{SCH}_2)\text{Re}$ were improved compared with that of the excited Ru units in $\text{Ru}(\text{CH}_2\text{CH}_2\text{CH}_2)\text{Re}$, likely because of the high electronegativities of the heteroatoms introduced into the bridging ligands. The increased quenching fraction should be partly responsible for improving the photocatalytic activity of $\text{Ru}(\text{CH}_2\text{OCH}_2)\text{Re}$. However, the quenching fraction of $\text{Ru}(\text{CH}_2\text{OCH}_2)\text{Re}$ increased only 1.2-fold compared with that of $\text{Ru}(\text{CH}_2\text{CH}_2\text{CH}_2)\text{Re}$, whereas the quantum yield of CO formation in the case of $\text{Ru}(\text{CH}_2\text{OCH}_2)\text{Re}$ increased by 1.7 times compared with that in the case of $\text{Ru}(\text{CH}_2\text{CH}_2\text{CH}_2)\text{Re}$. Other factors likely contribute to the improvement of the photocatalytic activity of $\text{Ru}(\text{CH}_2\text{OCH}_2)\text{Re}$. In addition, both the Φ_{CO} and TON_{CO} in the case of $\text{Ru}(\text{CH}_2\text{SCH}_2)\text{Re}$ were lower compared to those in the case of $\text{Ru}(\text{CH}_2\text{CH}_2\text{CH}_2)\text{Re}$, even though the η_q of $\text{Ru}(\text{CH}_2\text{SCH}_2)\text{Re}$ was greater than that of $\text{Ru}(\text{CH}_2\text{CH}_2\text{CH}_2)\text{Re}$.

Fig. 4 illustrates the cyclic voltammograms (CVs) of the diads measured in MeCN containing Et_4NBF_4 (0.1 M) as a supporting electrolyte. In the case of $\text{Ru}(\text{CH}_2\text{OCH}_2)\text{Re}$, as shown in Fig. 5a, five reduction waves were observed in the cathodic scan; these waves were respectively attributed, from left to right, to the ligand-based reduction of the Re unit, the first ligand-based reduction of the Ru unit, the second ligand-based reduction of the Ru unit, the Re-centered reduction, and the third ligand-based reduction of the Ru unit on the basis of comparison with the corresponding model complexes. All of the reduction waves

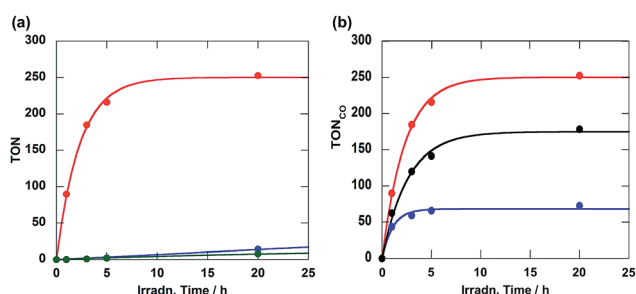


Fig. 2 (a) Turnover number of $\text{Ru}(\text{CH}_2\text{OCH}_2)\text{Re}$ for CO (red), HCOOH (green), and H_2 (blue) formation and (b) those of $\text{Ru}(\text{CH}_2\text{OCH}_2)\text{Re}$ (red), $\text{Ru}(\text{CH}_2\text{SCH}_2)\text{Re}$ (black), and $\text{Ru}(\text{CH}_2\text{CH}_2\text{CH}_2)\text{Re}$ (blue) for CO formation as a function of irradiation time. DMF–TEOA (5 : 1) solutions containing 0.05 mM of the diad and 0.1 M of BNAH were irradiated at $\lambda > 500$ nm under a CO_2 atmosphere.



Table 1 Emission properties of the metal complexes and quenching rates of the emission by BNAH^a

Complex	λ_{em}^a/nm	Φ_{em}^a	τ_{em}^a/ns	$k_q\tau^{b,c}/M^{-1} s^{-1}$	$k_q/10^7 M^{-1}$	η_q^d
Ru(CH₂OCH₂)Re	649	0.087	735	42.1	5.73	0.82
Ru(CH₂SCH₂)Re	649	0.087	734	36.3	4.95	0.78
Ru(CH₂CH₂CH₂)Re	639	0.097	761	21.0	2.76	0.67
Ru(CH₂OCH₂)Re(CO)₃(X) X = ⁻ OC(O)OC ₂ H ₄ N(C ₂ H ₄ OH) ₂	645	0.119 ^b	724 ^b	14.0	1.92	0.58
Ru	639	0.086	760	—	—	—
Ru(CH₂OCH₂)	649	0.092	747	—	—	—

^a DMF was used as the solvent, and the excitation wavelength was 456 nm. ^b DMF-TEOA (5 : 1 v/v) was used as the solvent. ^c The excitation wavelength was 520 nm. ^d Quenching fraction with 0.1 M BNAH, $\eta_q = 1 - 1/(1 + k_q\tau[BNAH])$.

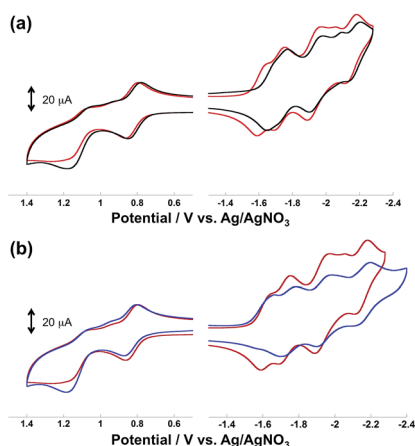


Fig. 4 Cyclic voltammograms of (a) Ru(CH₂OCH₂)Re (red) and Ru(CH₂CH₂CH₂)Re (black), and (b) Ru(CH₂SCH₂)Re (blue) and Ru(CH₂OCH₂)Re (red) measured in MeCN containing Et₄NBF₄ (0.1 M) as the supporting electrolyte.

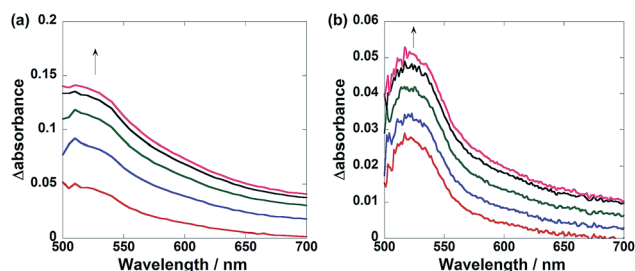


Fig. 5 *In situ* differential UV-vis absorption spectra of the reaction solutions before and after irradiation: (a) Ru(CH₂OCH₂)Re, where the irradiation time was 840–1080 s at intervals of 60 s; (b) Ru(CH₂CH₂CH₂)Re, where the irradiation time was 2640–2760 s at intervals of 30 s. DMF-TEOA (5 : 1) solutions containing BNAH (0.1 M) and the complex (0.3 mM) were irradiated under a CO₂ atmosphere at $\lambda = 480$ nm with a light intensity of 3.2×10^{-9} einsteins⁻¹.

except for the Re-centered reduction were reversible. In the anodic scan, two oxidation waves were observed, the reversible wave at $E_{1/2} = 0.82$ V and the irreversible wave at $E_p = 1.21$ V were attributed to the Ru-centered (Ru(II)/Ru(III)) and the Re-centered oxidation (Re(I)/Re(II)), respectively.

All redox waves in the CV of Ru(CH₂CH₂CH₂)Re were similarly observed but negatively shifted compared to those of Ru(CH₂OCH₂)Re (Fig. 4a). In the case of Ru(CH₂SCH₂)Re, however, the ligand-based reduction of the Re unit was irreversible and the Re-centered reduction wave could not be identified (Fig. 4b). This result suggests that the one-electron-reduced species (OERs) of Ru(CH₂SCH₂)Re was less stable than the corresponding OERs of the other diads. The first reduction waves of the Re units in both Ru(CH₂OCH₂)Re and Ru(CH₂CH₂CH₂)Re were observed at potentials similar to those of the corresponding model complexes, *i.e.*, Re(CH₂OCH₂) and Re (Table 2). This observation also indicates that the Ru unit did not exert a strong electronic effect on the Re units through the bridging ligand. Therefore, the positive shifts of the redox potentials of Ru(CH₂OCH₂)Re compared to those of Ru(CH₂CH₂CH₂)Re, as described above, are attributable mainly to the electron-withdrawing ability of the oxygen atom in the bridging ligand, which lowers the HOMO and LUMO energies of the Ru and Re units.

The first reduction of Ru(CH₂OCH₂) was observed at a potential 20 mV more positive than that of Ru; however, the first reduction of Re(CH₂OCH₂) was 50 mV more positive than that of Re (Table 2). This discrepancy indicates that the introduction of an oxygen atom into the bridging ligand more strongly affected the LUMO energy of the Re unit than that of the Ru unit and that, in the case of Ru(CH₂OCH₂)Re, the driving force of intramolecular electron transfer from the OERs of the Ru unit to the Re unit was greater than that of Ru(CH₂CH₂CH₂)Re.

These results are consistent with the differences between the UV-vis absorption spectra of the solutions during the photocatalytic reactions in the presence of Ru(CH₂OCH₂)Re and Ru(CH₂CH₂CH₂)Re (Fig. 5). In the case of Ru(CH₂CH₂CH₂)Re, a relatively sharp absorption band with a maximum at 520 nm appeared during irradiation (Fig. 5a). The corresponding absorption band of Ru(CH₂OCH₂)Re was broader, with relatively stronger absorption at wavelengths longer than ~ 560 nm (Fig. 5b). Both spectra were fitted by a linear combination of the absorption spectra of the OERs of Ru and Re, which were obtained by the flow electrolysis method (Fig. S2, ESI[†]). Using these data, we calculated the ratios of the OERs between the Ru and Re units to be 1 : 1.3 in the case of Ru(CH₂CH₂CH₂)Re, and 1 : 9.3 in the case of Ru(CH₂OCH₂)Re (Fig. S3, ESI[†]). These results strongly indicate that the added electron was more



Table 2 Electrochemical properties of the metal complexes

Complex	$E_{1/2}$ ($\Delta E/mV$)/V vs. Ag/AgNO ₃			$[Re(L/L^-)]$	$[Re^{0/I}]^a$	$[Ru^{II/III}]$	$[Re^{II/III}]^a$
	Ligand based reduction of the Ru unit						
Ru(CH₂OCH₂)Re	-1.73 (61)	-1.93 (103)	-2.15 (76)	-1.62 (66)	-2.00	+0.82 (70)	+1.21
Ru(CH₂SCH₂)Re	-1.73 (110)	-1.94 (100)	-2.15 (110)	-1.67 ^a	— ^b	+0.84 (70)	+1.19
Ru(CH₂CH₂CH₂)Re	-1.76 (50)	-1.94 (90)	-2.16 (92)	-1.67 (40)	-2.10	+0.81 (70)	+1.15
Ru(CH₂OCH₂)	-1.72 (73)	-1.91 (72)	-2.15 (70)			+0.84 (76)	
Ru^c	-1.74 (76)	-1.93 (71)	-2.16 (71)			+0.82 (67)	
Re(CH₂OCH₂)				-1.62 (60)	-2.12		+1.15
Re^c				-1.67 (65)	-2.22		+1.15

^a Peak potential of the irreversible wave. ^b The wave was not identified. ^c From ref. 8e.

localized on the Re unit in the OERs of **Ru(CH₂OCH₂)Re** than that of **Ru(CH₂CH₂CH₂)Re** because of the greater driving force of the intramolecular electron transfer from the Ru unit to the Re unit. This greater driving force should be another reason for the higher photocatalytic efficiency of **Ru(CH₂OCH₂)Re**.

Fig. 6 illustrates size-exclusion chromatograms of the reaction solution in the case of **Ru(CH₂OCH₂)Re**. Before irradiation, only a single peak attributed to **Ru(CH₂OCH₂)Re** was observed at 34.9 min. The irradiation induced a decrease in the intensity of the peak of **Ru(CH₂OCH₂)Re** with the appearance of a new peak at 36.1 min; after 120 min of irradiation, a photostationary state, where the ratio of the peak areas was approximately 3 : 1, was observed. The electrospray ionization (ESI) mass spectra of the eluents collected at 36.1 min showed a peak attributable to $[(dmb)_2Ru(CH_2OCH_2)Re(CO)_3(CH_3COO^-)]^{2+}$, whose CH_3COO^- group likely originated from the eluent (MeCN–MeOH (1 : 1 v/v) containing 0.05 M CH_3COONH_4) at $m/z = 591$ (Fig. S4, ESI[†]). This result strongly suggests that the Re unit in some **Ru(CH₂OCH₂)Re** complexes was converted into a tricarbonyl complex, *i.e.*, $fac-[Re(N^{\wedge}N)(CO)_3(L)]$ ($N^{\wedge}N$ = diimine ligand, L = monodentate ligand), during the first stage of the photocatalytic reaction.

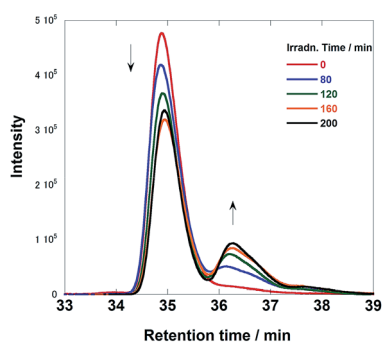


Fig. 6 Size exclusion chromatograms of the solutions before and after the photocatalytic reaction using **Ru(CH₂OCH₂)Re** (irradiation times: 0, 80, 120, 160, and 200 min). The eluent was MeCN–MeOH (1 : 1 v/v) containing 0.5 M CH_3COONH_4 ; two Shodex PROTEIN KW402.5 columns were used with a KW-LG guard column under the following conditions: flow rate, 0.2 mL min⁻¹; column temperature, 40 °C; detection wavelength, 390 nm. The reaction conditions were the same as those described in Fig. 5.

Fig. 7 shows *in situ* IR spectral changes of a solution during the photocatalytic reaction. The concentration of the diad was greater than that used in the case of Fig. 6 because of the lower sensitivity of the IR spectrometer compared to that of the size exclusion chromatograph. Immediately after the irradiation was initiated, the CO-stretching bands corresponding to the Re unit of **Ru(CH₂OCH₂)Re** ($\nu_{CO} = 1938$ and 1868 cm⁻¹) decreased in intensity, whereas a pair of bands of the corresponding OERs ($\nu_{CO} = 1909$ and 1836 cm⁻¹) increased in intensity.¹⁰ Further irradiation resulted in the formation of new bands attributable to two kinds of diads with a Re tricarbonyl unit ($\nu_{CO} = 2018$, 2006, and ~ 1890 cm⁻¹; other ν_{CO} bands associated with these species should be observed, but they were overlapped by the bands of other species). These species were identified as diads with two types of the Re units: $fac-[Re(N^{\wedge}N)(CO)_3\{OC_2H_4N(C_2H_4OH)_2\}]$ with a deprotonated TEOA ligand, and its CO₂-inserted product, $fac-[Re(N^{\wedge}N)(CO)_3\{OC(O)OC_2H_4N(C_2H_4OH)_2\}]$, where both TEOA and CO₂ molecules are captured to form a carbonate ester ligand. These structural assignments are based on the similarities of these species to the corresponding Re mononuclear complexes, *i.e.*, $fac-[Re(bpy)(CO)_3\{OC_2H_4N(C_2H_4OH)_2\}]$ ($\nu_{CO} = 2006$, 1897, 1881 cm⁻¹) and $fac-[Re(bpy)(CO)_3\{OC(O)OC_2H_4N(C_2H_4OH)_2\}]$ ($\nu_{CO} = 2020$, 1915, 1892 cm⁻¹) (bpy = 2,2'-bipyridine), reported in our previous paper.¹¹ As described below, the IR spectra of authentic samples of the diads with either a $^-OC_2H_4N(C_2H_4OH)_2$ or a $^-OC(O)OC_2H_4N(C_2H_4OH)_2$ ligand, *i.e.*, **Ru(CH₂OCH₂)Re(CO)₃(X)** (X = $^-OC_2H_4N(C_2H_4OH)_2$

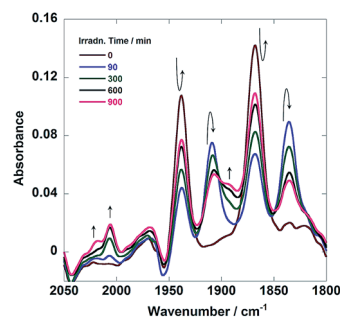
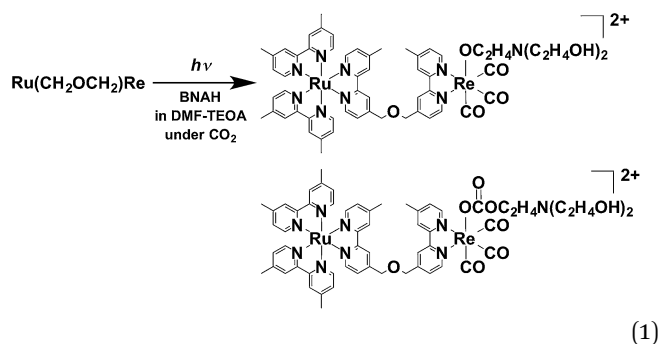


Fig. 7 *In situ* IR spectra of a DMF–TEOA (5 : 1 v/v) solution containing **Ru(CH₂OCH₂)Re** (1 mM) and BNAH (0.1 M) during photoirradiation at $\lambda = 480$ nm under a CO₂ atmosphere.



or ${}^{-}\text{OC}(\text{O})\text{OC}_2\text{H}_4\text{N}(\text{C}_2\text{H}_4\text{OH})_2$) also showed similar CO-stretching bands (Fig. S5, ESI †). These results strongly indicate that $\text{Ru}(\text{CH}_2\text{OCH}_2)\text{Re}$ was partially converted into $\text{Ru}(\text{CH}_2\text{OCH}_2)\text{Re}(\text{CO})_3(\text{X})$ in the first stage of the photocatalytic reaction (eqn (1)).



Further irradiation resulted in a photostationary state, where the reaction solution contained both $\text{Ru}(\text{CH}_2\text{OCH}_2)\text{Re}$ and $\text{Ru}(\text{CH}_2\text{OCH}_2)\text{Re}(\text{CO})_3(\text{X})$ in an approximately 3 : 1 ratio, as described above. Fig. 8 illustrates the initial stage of photocatalytic CO formation at lower light intensity (3.2×10^{-9} einstein s^{-1}) than that used in the case of Fig. 2. An induction period of CO formation was observed in the case of $\text{Ru}(\text{CH}_2\text{OCH}_2)\text{Re}$, which strongly indicates that $\text{Ru}(\text{CH}_2\text{OCH}_2)\text{Re}(\text{CO})_3(\text{X})$ played an important role in the photocatalytic reaction. Therefore, we synthesized $\text{Ru}(\text{CH}_2\text{OCH}_2)\text{Re}(\text{CO})_3(\text{X})$ by reacting $\text{Ru}(\text{CH}_2\text{OCH}_2)\text{Re}(\text{CO})_3(\text{MeCN})$, TEOA, and CO_2 ¹¹ and investigated the photocatalytic ability of $\text{Ru}(\text{CH}_2\text{OCH}_2)\text{Re}(\text{CO})_3(\text{X})$; the results are also shown in Fig. 8 (green). The clear induction period of CO formation disappeared; however, the quantum yield of CO formation ($\Phi_{\text{CO}} = 0.12$) was lower than that achieved with $\text{Ru}(\text{CH}_2\text{OCH}_2)\text{Re}$ ($\Phi_{\text{CO}} = 0.18$, red in Fig. 8). Given these results, we examined the photocatalytic ability of a 3 : 1 mixed system of $\text{Ru}(\text{CH}_2\text{OCH}_2)\text{Re}$ and $\text{Ru}(\text{CH}_2\text{OCH}_2)\text{Re}(\text{CO})_3(\text{X})$, which is a similar ratio observed in the photostationary state when only $\text{Ru}(\text{CH}_2\text{OCH}_2)\text{Re}$ was used as the photocatalyst (Fig. 6). As shown in Fig. 8 (orange), no clear induction period

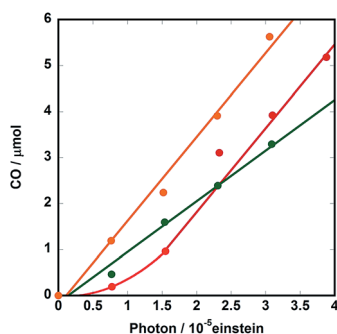


Fig. 8 Photocatalytic CO formation using DMF-TEOA (5 : 1 v/v) solutions containing 0.1 M of BNAH and 0.3 mM of $\text{Ru}(\text{CH}_2\text{OCH}_2)\text{Re}$ (red), $\text{Ru}(\text{CH}_2\text{OCH}_2)\text{Re}(\text{CO})_3(\text{X})$ (green), or a 3 : 1 mixture of $\text{Ru}(\text{CH}_2\text{OCH}_2)\text{Re}$ and $\text{Ru}(\text{CH}_2\text{OCH}_2)\text{Re}(\text{CO})_3(\text{X})$ (orange). The reaction conditions were same as those described in Fig. 5.

was observed and the quantum yield of CO formation achieved using this system ($\Phi_{\text{CO}} = 0.19$) was similar to that achieved using $\text{Ru}(\text{CH}_2\text{OCH}_2)\text{Re}$ after the induction period ($\Phi_{\text{CO}} = 0.18$). Therefore, we conclude that $\text{Ru}(\text{CH}_2\text{OCH}_2)\text{Re}$ and $\text{Ru}(\text{CH}_2\text{OCH}_2)\text{Re}(\text{CO})_3(\text{X})$ played important but different roles in the photocatalytic reaction.

Fig. 9 illustrates the rise and decay curves of the FT-IR absorption peaks (Fig. 7) attributed to each diad in the reaction solution during irradiation. However, immediately after the irradiation was started, the OERs of the Re unit in $\text{Ru}(\text{CH}_2\text{OCH}_2)\text{Re}$ (blue) formed rapidly and its concentration decreased between 120 s and 600 s of irradiation time, the non-reduced $\text{Ru}(\text{CH}_2\text{OCH}_2)\text{Re}$ (red) was recovered. Further irradiation did not induce a change in the ratio between the OERs and non-reduced species. The decrease of the concentration of the OERs appeared to occur after $\text{Ru}(\text{CH}_2\text{OCH}_2)\text{Re}(\text{CO})_3(\text{X})$ (green and purple) was accumulated in the reaction solution. These results indicate that efficient electron transfer from the OERs of $\text{Ru}(\text{CH}_2\text{OCH}_2)\text{Re}$ to $\text{Ru}(\text{CH}_2\text{OCH}_2)\text{Re}(\text{CO})_3(\text{X})$ and/or an intermediate produced from the OERs of $\text{Ru}(\text{CH}_2\text{OCH}_2)\text{Re}(\text{CO})_3(\text{X})$ occurred during the steady-state CO formation in the photocatalytic reaction.

Scheme 1 summarizes the possible mechanism for the photocatalytic reaction involving $\text{Ru}(\text{CH}_2\text{OCH}_2)\text{Re}$. The Ru unit is selectively excited, and the resulting ${}^3\text{MLCT}$ excited state is reductively quenched by BNAH to give the OER species of the Ru unit of $\text{Ru}(\text{CH}_2\text{OCH}_2)\text{Re}$. Rapid intramolecular electron transfer proceeds from the OERs of the Ru unit to the Re unit to give the OER species of the Re unit of $\text{Ru}(\text{CH}_2\text{OCH}_2)\text{Re}$. Rapid abstraction of a proton from the one-electron-oxidized BNAH by TEOA and dimerization have been reported to proceed to give BNA_2 . In the first stage of the photocatalytic reaction, approximately a quarter of the added $\text{Ru}(\text{CH}_2\text{OCH}_2)\text{Re}$ was efficiently converted into $\text{Ru}(\text{CH}_2\text{OCH}_2)\text{Re}(\text{CO})_3(\text{X})$ ($\text{X} = {}^{-}\text{OC}_2\text{H}_4\text{N}(\text{C}_2\text{H}_4\text{OH})_2$ or ${}^{-}\text{OC}(\text{O})\text{OC}_2\text{H}_4\text{N}(\text{C}_2\text{H}_4\text{OH})_2$), which was the real photocatalyst for CO_2 reduction. $\text{Ru}(\text{CH}_2\text{OCH}_2)\text{Re}$, which remained in the solution, functioned as a redox photosensitizer that supplied electrons to $\text{Ru}(\text{CH}_2\text{OCH}_2)\text{Re}(\text{CO})_3(\text{X})$ and/or the intermediate during the photocatalytic reaction. Notably, the

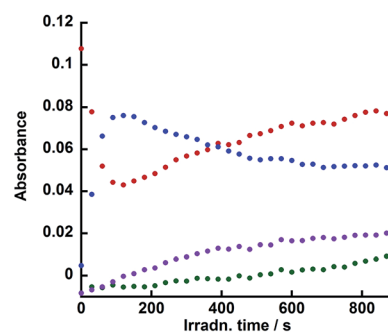


Fig. 9 Changes in the intensities of the absorbance peaks in the *in situ* IR spectra (Fig. 7): $\text{Ru}(\text{CH}_2\text{OCH}_2)\text{Re}(\text{CO})_3(\text{X})$ (green, 2018 cm^{-1} , $\text{X} = {}^{-}\text{OC}(\text{O})\text{OC}_2\text{H}_4\text{N}(\text{C}_2\text{H}_4\text{OH})_2$); purple, 2006 cm^{-1} , $\text{X} = {}^{-}\text{OC}_2\text{H}_4\text{N}(\text{C}_2\text{H}_4\text{OH})_2$), $\text{Ru}(\text{CH}_2\text{OCH}_2)\text{Re}$ (red, 1938 cm^{-1}), and the OER species of $\text{Ru}(\text{CH}_2\text{OCH}_2)\text{Re}$ (blue, 1909 cm^{-1}). See Fig. 7.



Ru unit of $\text{Ru}(\text{CH}_2\text{OCH}_2)\text{Re}(\text{CO})_3(\text{X})$ should serve as another redox photosensitizer (Table 1, Fig. S6, ESI†) because $\text{Ru}(\text{CH}_2\text{OCH}_2)\text{Re}(\text{CO})_3(\text{X})$ alone can function as a relatively efficient photocatalyst for CO_2 reduction, though its Φ_{CO} is lower than that of the mixed system. Because the absorption band attributable to the OER species of $\text{Ru}(\text{CH}_2\text{OCH}_2)\text{Re}(\text{CO})_3(\text{X})$ was not detected in the UV-vis absorption spectrum of the reaction solution during the photocatalytic reaction, the photochemically accepted electron in the Ru unit should rapidly transfer to the Re unit and then participate in the reduction of CO_2 . The electrons for the second reduction process, where an electron was accepted by the Re unit of the intermediate forming from the OER species of $\text{Ru}(\text{CH}_2\text{OCH}_2)\text{Re}(\text{CO})_3(\text{X})$ to produce CO, originated from two possible sources: the reduced Ru unit in the intermediate or the reduced $\text{Ru}(\text{CH}_2\text{OCH}_2)\text{Re}$. The previously described results indicate that the reduction efficiency with the latter species was better than that with the former species; *i.e.*, the reduction of the intermediate should be a rate-limiting process in the photocatalytic reduction of CO_2 *via* $\text{Ru}(\text{CH}_2\text{OCH}_2)\text{Re}(\text{CO})_3(\text{X})$ under the investigated reaction conditions. Because similar photocatalytic behavior of $\text{Ru}(\text{CH}_2\text{CH}_2\text{CH}_2)\text{Re}$ was observed (Fig. S7–S9, ESI†), the photocatalytic reaction involving $\text{Ru}(\text{CH}_2\text{CH}_2\text{CH}_2)\text{Re}$ should proceed through a mechanism similar to that for $\text{Ru}(\text{CH}_2\text{OCH}_2)\text{Re}$.

As previously described, the durability of $\text{Ru}(\text{CH}_2\text{SCH}_2)\text{Re}$ was much lower than that observed for the other diads. Fig. 10 shows SEC analysis data of the reaction solution; these chromatograms clearly indicate that $\text{Ru}(\text{CH}_2\text{SCH}_2)\text{Re}$ completely disappeared after irradiation for 80 min and that two new species with smaller sizes formed. The LC-MS analysis data (Fig. S10, ESI†) indicated that the species detected at retention times of 36.5 min and 37.8 min were Ru(II) mononuclear complexes, *i.e.*, $\text{Ru}(\text{CH}_2\text{OCH}_2)$, Ru , and $[\text{Ru}(\text{dmb})_2(\text{CS}^-)]^+$ ($\text{CS}^- = \text{MebpyCH}_2\text{S}^-$), and Re(I) mononuclear complexes, *i.e.*, Re , $[\text{Re}(\text{CH}_2\text{OCH}_2)(\text{CO})_2\{\text{P}(p\text{-FPh}_3)_2\}_2]^+$, and $[\text{Re}(\text{dmb})(\text{CO})_2\{\text{P}(p\text{-FPh}_3)_3\}(\text{MeCN})]^+$ (MeCN was contained in the eluent), respectively. Therefore, $\text{Ru}(\text{CH}_2\text{SCH}_2)\text{Re}$ was completely cleaved to give the mononuclear complexes in the first stage of the reaction, which should lower both the efficiency and durability of the photocatalysis of $\text{Ru}(\text{CH}_2\text{SCH}_2)\text{Re}$.

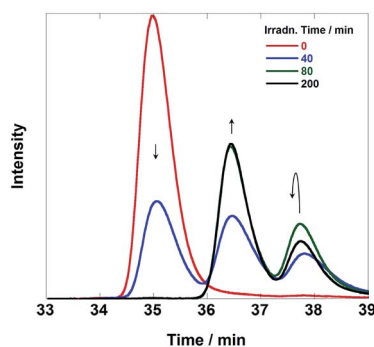


Fig. 10 Size exclusion chromatograms of the solutions before and after the photocatalytic reaction using $\text{Ru}(\text{CH}_2\text{SCH}_2)\text{Re}$ (irradiation times: 0, 40, 80, and 200 min). The reaction and analytical conditions were the same as those described in Fig. 6.

Experimental

General procedures

UV-vis absorption spectra were recorded on a JASCO V-565 spectrophotometer. ^1H NMR spectra were recorded on a JEOL AL300 (300 MHz) spectrometer. The residual proton of the deuterated solvent (acetone- d_6 or acetonitrile- d_3) was used as an internal standard. Emission spectra were measured at 25 ± 0.1 °C under an Ar atmosphere using a JASCO FP-6500 spectrofluorometer. Emission quantum yields were obtained with a Hamamatsu photonics C-9920-02 integrating sphere and a multi-photodiode-array detector. Emission lifetimes were measured with a Horiba FluoroCube time-correlated single-photon counting system (the excitation source was an LED pulse lamp (456 nm) with an instrumental response time of less than 0.1 ns). In the quenching experiments, the changes in the emission intensities of solutions containing a complex were monitored in the presence of various amounts of the quencher, BNAH. Quenching rate constants (k_q) were calculated from linear Stern–Volmer plots. Electrospray ionization-mass spectroscopy (ESI-MS) was recorded on a Shimadzu LCMS-2010A mass spectrometer using MeCN or MeOH as the mobile phase. The redox potentials of the complexes in a MeCN solution were measured using a cyclic voltammetric technique. The CVs were recorded on an ALS/CHI CHI-620 electrochemical analyzer using Et_4NBF_4 (0.1 M) as the supporting electrolyte, a glassy-carbon disk working electrode (3 mm diameter), an Ag/AgNO₃ (0.01 M) reference electrode, and a Pt counter electrode. The scan rate was 200 mV s^{-1} . Analytical SEC¹² was conducted using an HPLC system consisting of a JASCO 880-PU pump, a pair of Shodex PROTEIN KW402.5 columns, a KW-LG guard column, a Rheodyne 7125 injector, and a JASCO MD-2010 plus UV-Vis photodiode-array detector. The column temperature was maintained at 40 °C using a JASCO 860-CO column oven. A mixed solution of MeCN–MeOH (1 : 1 v/v) containing $\text{CH}_3\text{COONH}_4$ (0.5 mM) was used as the mobile phase. In the case of HPLC(SEC)-MS analyses, a HPLC system consisting of the SEC columns and the guard column, a Rheodyne 7125 injector, a Shimadzu FCV-10ALVP gradient unit, and a Shimadzu LC-10ADVP pump was connected before the ESI-MS detector. The column temperature was maintained at 40 °C using a Shimadzu SPD CTO-10ACVP oven. A MeCN–MeOH (1 : 1 v/v) mixed solution containing $\text{CH}_3\text{COONH}_4$ (0.05 mM) was used as the mobile phase. Isolation of the diads was achieved by preparative SEC using a pair of Shodex PROTEIN KW 2002.5 columns, a KW-LG guard column, and a JAI LC-9201 recycling preparative HPLC apparatus with a JASCO 870-UV detector. A MeCN–MeOH (1 : 1 v/v) mixed solution containing $\text{CH}_3\text{COONH}_4$ (0.15 mM) was used as the mobile phase.

Photocatalytic reactions

Photocatalytic reactions were performed on a 4 mL DMF–TEOA (5 : 1 v/v) mixed solution containing the diad (0.05 mM) and BNAH (0.1 M) in an 11 mL test tube (*i.d.* 8 mm). After the solution was purged with CO_2 for 15 min, it was irradiated in a



merry-go-round irradiation apparatus using $\lambda > 500$ nm light from a high-pressure Hg lamp equipped with a uranyl glass and a K_2CrO_4 (30% w/w, light pass length: 1 cm) solution filter. The tube was cooled with tap water during irradiation. In the case of quantum yield measurements, the mixed solution containing a higher concentration of the diad (0.3 mM) in a quartz cubic cell (the light pass length: 1 cm) was irradiated using a 480 nm monochromic light from an Ushio UXL-500D-O xenon short-arc lamp equipped with a 480 nm (FWHM: 10 nm) band-pass filter (Asahi Spectra Co.) and a CuSO_4 solution filter (250 g L^{-1} , light pass length: 5 cm). The absorbance of the reaction solution (>3 at 480 nm) during the measurement indicated that most of the irradiated light was absorbed by the diad in the solution. The temperature of the solutions was controlled during irradiation at 25 ± 0.1 °C using an IWAKI CTS-134A constant-temperature system. The incident light intensity was determined using a $\text{K}_3\text{Fe}(\text{C}_2\text{O}_4)_3$ actinometer.¹³ The gaseous products, *i.e.*, CO and H_2 , were analyzed by GC-TCD (GL Science GC323), and the liquid-phase product, *i.e.*, HCOOH, was analyzed by a capillary electrophoresis system (Otsuka Electronics Co. Capi-33001).

Materials

Acetonitrile was distilled over P_2O_5 three times and then distilled over CaH_2 immediately before use. DMF was dried over molecular sieves 4A and then distilled under reduced pressure (10–20 mmHg). TEOA was distilled under reduced pressure (<1 mmHg). DMF and TEOA were stored under an Ar atmosphere prior to use. Et_4NBF_4 was dried under vacuum at 100 °C for a day prior to use. All other reagents were reagent-grade quality and were used without further purification. BNAH,¹⁴ the bridging ligands (4'-methyl-[2,2'-bipyridine]-4-yl)- CH_2XCH_2 - (4'-methyl-[2,2'-bipyridine]-4-yl): X = O (CH_2OCH_2);¹⁵ S (CH_2SCH_2);¹⁵ CH_2 ($\text{CH}_2\text{CH}_2\text{CH}_2$),¹⁶ $\text{Ru}(\text{dmb})_2\text{Cl}_2$,¹⁷ and *mer*- $[\text{Re}(\text{CO})_3\{\text{P}(p\text{-FPh}_3)\}_2\text{Br}]$ ¹⁸ were synthesized according to the methods described in the literature.

Synthetic procedures

Synthesis of $[\text{Re}(\text{CO})_2\{\text{P}(p\text{-FPh}_3)\}_2(\text{CH}_2\text{OCH}_2)](\text{PF}_6)_3 \cdot 3\text{H}_2\text{O}$ ($\text{Re}(\text{CH}_2\text{OCH}_2)$). A THF solution (17 mL) containing *mer*- $[\text{Re}(\text{CO})_3\{\text{P}(p\text{-FPh}_3)\}_2\text{Br}]$ (197 mg, 0.200 mmol) and AgOTf (54.0 mg, 0.210 mmol) was refluxed for 3 h under an N_2 atmosphere in the absence of light. After the mixture had cooled to room temperature, the white precipitate was removed by filtration through Celite. After evaporation of the solvent, CH_2OCH_2 (229 mg, 0.599 mmol) was added to the residue and the mixture was dissolved in EtOH (60 mL). The solution was refluxed for 5 h under an N_2 atmosphere in the absence of light. After evaporation of the solvent, the by-products were removed by column chromatography on an SP Sephadex C-25 ion-exchange column using $\text{MeCN-H}_2\text{O}$ (1 : 1 v/v) containing NH_4PF_6 as the eluent and then by preparative SEC. Purification of the product was achieved by recrystallization using a $\text{MeOH-H}_2\text{O}$ mixed solvent. The yield was 32% (91 mg, 0.065 mmol). Elemental analysis calcd (%) for $\text{C}_{62}\text{H}_{52}\text{F}_{12}\text{N}_4\text{O}_6\text{P}_3\text{Re}$: C. 51.14; H. 3.60; N. 3.85, found: C. 51.18; H. 3.50; N. 3.89. $^1\text{H-NMR}$ (300 MHz, acetone- d_6) δ/ppm : 8.68 (d, $J = 4.8$ Hz, 1H, β -bpy-6), 8.51 (s, 1H, γ -bpy-3),

8.49 (d, $J = 4.4$ Hz, 1H, α -bpy-6), 8.41 (s, 1H, β -bpy-3), 8.35 (s, 1H, δ -bpy-3), 8.28 (s, 1H, α -bpy-3), 8.19 (d, $J = 4.8$ Hz, 1H, γ -bpy-6), 8.07 (d, $J = 3.6$ Hz, 1H, δ -bpy-6), 7.44 (d, $J = 4.8$ Hz, 1H, β -bpy-5), 7.38–7.32 (m, 12H, Ph-o), 7.28–7.23 (m, 2H, α -bpy-5, γ -bpy-5), 7.12 (t, $J_{\text{HH}} = 8.4$ Hz, $J_{\text{FH}} = 8.4$ Hz, 12H, Ph-m), 7.07 (d, $J = 5.6$ Hz, 1H, δ -bpy-5), 4.84 (s, 2H, β - CH_2), 4.82 (s, 2H, γ - CH_2), 2.46 (s, 6H, α -bpy- CH_3 , δ -bpy- CH_3). FT-IR (in CH_2Cl_2) $\nu_{\text{CO}}/\text{cm}^{-1}$: 1868, 1939. ESI-MS (eluent: MeCN) m/z : 629 ($[\text{M} - \text{PF}_6^- + \text{H}^+]^{2+}$), 944 ($[\text{M} - \text{P}(p\text{-FPh}_3)_3 - \text{PF}_6^-]^{+}$).

Synthesis of $[(\text{dmb})_2\text{Ru}(\text{CH}_2\text{OCH}_2)](\text{PF}_6)_2 \cdot \text{H}_2\text{O}$ ($\text{Ru}(\text{CH}_2\text{OCH}_2)$). An EtOH- H_2O (40 mL and 10 mL) mixed solution containing $\text{Ru}(\text{dmb})_2\text{Cl}_2$ (91.5 mg, 0.159 mmol) and CH_2OCH_2 (184 mg, 0.482 mmol) was refluxed for 8 h under an N_2 atmosphere in the absence of light. After evaporation of the solvent, water was added to the residue, giving a white precipitate of CH_2OCH_2 ; this precipitate was removed by filtration. NH_4PF_6 was added to the filtrate to give precipitates, which were recovered by filtration and washed with H_2O . The product was isolated by column chromatography on an SP Sephadex C-25 ion-exchange column using $\text{MeCN-H}_2\text{O}$ (1 : 1 v/v) containing NH_4PF_6 as the eluent; the product was subsequently recrystallized from a CH_2Cl_2 -ether mixed solvent. The yield was 88% (160 mg, 0.14 mmol). Elemental analysis calcd (%) for $\text{C}_{48}\text{H}_{48}\text{F}_{12}\text{N}_8\text{O}_2\text{P}_2\text{Ru}$: C. 49.70; H. 4.17; N. 9.66, found: C. 49.66; H. 4.13; N. 9.59. $^1\text{H-NMR}$ (300 MHz, acetone- d_6) δ/ppm : 8.78 (s, 1H, β -bpy-3), 8.66 (s, 5H, dmb-3, α -bpy-3), 8.62 (d, $J = 4.5$ Hz, 1H, γ -bpy-6), 8.48–8.46 (m, 2H, δ -bpy-6, γ -bpy-3), 8.31 (s, 1H, δ -bpy-3), 7.98 (d, $J = 5.7$ Hz, 1H, β -bpy-6), 7.85–7.81 (m, 5H, α -bpy-6, dmb-6), 7.57 (d, $J = 4.2$ Hz, 1H, β -bpy-5), 7.42–7.35 (m, 6H, γ -bpy-5, dmb-5, α -bpy-5), 7.25 (d, $J = 4.8$ Hz, 1H, δ -bpy-5), 4.92 (s, 2H, β - CH_2), 4.85 (s, 2H, γ - CH_2), 2.55–2.43 (m, 18H, dmb- CH_3 , α -bpy- CH_3 , δ -bpy- CH_3). ESI-MS (eluent: MeCN) m/z : 426 ($[\text{M} - 2\text{PF}_6^-]^{2+}$).

The other mononuclear complexes ($\text{Ru}(\text{CH}_2\text{SCH}_2)$ and $\text{Ru}(\text{CH}_2\text{CH}_2\text{CH}_2)$) were synthesized in a manner similar to that used for $\text{Ru}(\text{CH}_2\text{OCH}_2)$ but with CH_2SCH_2 or $\text{CH}_2\text{CH}_2\text{CH}_2$ used instead of CH_2OCH_2 as the bridging ligand.

$[(\text{dmb})_2\text{Ru}(\text{CH}_2\text{SCH}_2)](\text{PF}_6)_2$ ($\text{Ru}(\text{CH}_2\text{SCH}_2)$). Yield 44%. $^1\text{H-NMR}$ (300 MHz, acetone- d_6) δ/ppm : 8.60 (s, 4H, dmb-3), 8.47 (s, 1H, β -bpy-3), 8.36 (d, $J = 5.2$ Hz, 1H, γ -bpy-6), 8.34 (s, 1H, γ -bpy-3), 8.29 (d, $J = 4.9$ Hz, 1H, δ -bpy-6), 8.26 (s, 1H, α -bpy-3), 8.11 (s, 1H, δ -bpy-3), 7.81 (d, $J = 5.9$ Hz, 1H, β -bpy-6), 7.76–7.71 (m, 5H, dmb-6, α -bpy-6), 7.46 (d, $J = 5.9$ Hz, 1H, β -bpy-5), 7.41–7.25 (m, 6H, α -bpy-5, dmb-5, γ -bpy-5), 7.17 (d, $J = 4.2$ Hz, 1H, δ -bpy-5), 3.94–3.78 (m, 4H, β - CH_2 , γ - CH_2), 2.53–2.33 (m, 18H, dmb- CH_3 , α -bpy- CH_3 , δ -bpy- CH_3). ESI-MS (eluent: MeCN) m/z : 434 ($[\text{M} - 2\text{PF}_6^-]^{2+}$).

$[(\text{dmb})_2\text{Ru}(\text{CH}_2\text{CH}_2\text{CH}_2)](\text{PF}_6)_2$ ($\text{Ru}(\text{CH}_2\text{CH}_2\text{CH}_2)$). Yield 34%. $^1\text{H-NMR}$ (300 MHz, acetone- d_6) δ/ppm : 8.67 (s, 1H, β -bpy-3), 8.64 (s, 4H, dmb-3), 8.62 (s, 1H, α -bpy-3), 8.52 (d, $J = 5.0$ Hz, 1H, γ -bpy-6), 8.47 (d, $J = 5.0$ Hz, 1H, δ -bpy-6), 8.29 (s, 2H, γ -bpy-3, δ -bpy-3), 7.86–7.80 (m, 6H, α -bpy-6, β -bpy-6, dmb-6), 7.45 (d, $J = 5.5$ Hz, 1H, β -bpy-5), 7.38–7.36 (m, 5H, α -bpy-5, dmb-5), 7.29–7.25 (m, 2H, γ -bpy-5, δ -bpy-5), 3.00–2.81 (m, 4H, β - CH_2 , γ - CH_2), 2.55–2.43 (m, 18H, dmb- CH_3 , α -bpy- CH_3 , δ -bpy- CH_3), 2.16 (tt, 4H, $J = 4.6$ Hz, 4.6 Hz, $-\text{CH}_2-\text{CH}_2-\text{CH}_2-$). ESI-MS (eluent: MeCN) m/z : 426 ($[\text{M} - 3\text{PF}_6^-]^{3+}$).

$[(\text{dmb})_2\text{Ru}(\text{CH}_2\text{OCH}_2)\text{Re}\{\text{P}(p\text{-FPh}_3)\}_2](\text{PF}_6)_3$ ($\text{Ru}(\text{CH}_2\text{OCH}_2)\text{Re}$). A THF solution (30 ml) containing *mer*- $[\text{Re}(\text{CO})_3\{\text{P}(p\text{-FPh}_3)\}_2\text{Br}]$



(86.5 mg, 0.0880 mmol) and AgOTf (23.7 mg, 0.0924 mmol) was refluxed for 4 h under an N₂ atmosphere in the absence of light. After the mixture had cooled to room temperature, white precipitates were removed by filtration through Celite. After evaporation of the solvent, **Ru(CH₂OCH₂)** (51.4 mg, 0.0450 mmol) was added to the residue, and the mixture was dissolved in EtOH (60 mL). The solution was refluxed for 15 h under an N₂ atmosphere in the absence of light. After evaporation of the solvent, the product was purified by column chromatography on a CM Sephadex C-25 ion-exchange column using MeCN–H₂O (1 : 1 v/v) containing NH₄PF₆ as the eluent; the product was subsequently recrystallized with CH₂Cl₂–ether mixed solvent. The yield was 36% (35 mg, 0.016 mmol). Elemental analysis calcd (%) for C₈₆H₇₀F₂₄N₈O₃P₅ReRu: C, 47.78; H, 3.26; N, 5.18. Found: C, 47.52; H, 3.36; N, 5.16. ¹H-NMR (300 MHz, acetone-*d*₆) δ/ppm: 8.72 (s, 1H, β-bpy-3), 8.62 (s, 5H, α-bpy-3, dmb-3), 8.29 (s, 1H, γ-bpy-3), 8.20 (s, 1H, δ-bpy-3), 8.05 (d, *J* = 5.6 Hz, 1H, γ-bpy-6), 7.93 (d, *J* = 5.6 Hz, 1H, β-bpy-6), 7.90 (d, *J* = 5.6 Hz, 1H, δ-bpy-6), 7.81–7.79 (m, 5H, α-bpy-6, dmb-6), 7.55 (d, *J* = 5.6 Hz, 1H, β-bpy-5), 7.35–7.27 (m, 17H, α-bpy-5, dmb-5, Ph-*o*), 7.18 (d, *J* = 5.6 Hz, 1H, γ-bpy-5), 7.06 (dd, *J*_{HH} = 7.8 Hz, *J*_{FH} = 7.8 Hz, 12H, Ph-*m*), 6.97 (d, *J* = 5.2 Hz, 1H, δ-bpy-5), 4.86 (s, 2H, β-CH₂), 4.82 (s, 2H, γ-CH₂), 2.54–2.44 (m, 18H, dmb-CH₃, α-bpy-CH₃, δ-bpy-CH₃). FT-IR (in CH₂Cl₂) ν_{CO}/cm⁻¹: 1870, 1940. ESI-MS (eluent: MeCN) *m/z*: 576 ([M – 3PF₆⁻]³⁺), 936 ([M – 2PF₆⁻]²⁺).

The other diad was synthesized in a manner similar to that used to prepare **Ru(CH₂OCH₂)Re** but with **Ru(CH₂SCH₂)** or **Ru(CH₂CH₂CH₂)** used instead of **Ru(CH₂OCH₂)**.

Yield 19%. Elemental analysis calcd (%) for C₈₆H₇₂F₂₄N₈O₃P₅ReRuS: C, 47.04; H, 3.31; N, 5.10; S, 1.46. Found: C, 47.04; H, 3.45; N, 5.09; S, 1.68. ¹H-NMR (300 MHz, acetone-*d*₆) δ/ppm: 8.76 (s, 1H, γ-bpy-3), 8.66 (s, 5H, β-bpy-3, dmb-3), 8.33 (s, 1H, δ-bpy-3), 8.26 (s, 1H, α-bpy-3), 8.11 (d, *J* = 5.6 Hz, 1H, γ-bpy-6), 7.96 (d, *J* = 5.6 Hz, 1H, β-bpy-6), 7.89–7.81 (m, 6H, α-bpy-6, dmb-6, δ-bpy-6), 7.53 (d, *J* = 6.0 Hz, 1H, β-bpy-5), 7.39–7.29 (m, 17H, α-bpy-5, dmb-5, Ph-*o*), 7.17 (d, *J* = 5.6 Hz, 1H, γ-bpy-5), 7.10 (dd, *J*_{HH} = 8.6 Hz, *J*_{FH} = 8.4 Hz, 12H, Ph-*m*), 6.99 (d, *J* = 5.6 Hz, 1H, δ-bpy-5), 3.94–3.88 (m, 4H, β-CH₂, γ-CH₂), 2.57–2.54 (m, 18H, dmb-CH₃, α-bpy-CH₃, δ-bpy-CH₃). FT-IR (in CH₂Cl₂) ν_{CO}/cm⁻¹: 1868, 1939. ESI-MS (eluent: MeCN) *m/z*: 581 ([M – 3PF₆⁻]³⁺), 944 ([M – 2PF₆⁻]²⁺).

[(dmb)₂Ru(CH₂CH₂CH₂)Re{P(*p*-FPh)₃}]₂(PF₆)₃ (Ru(CH₂CH₂CH₂)Re). Yield 72%. Elemental analysis calcd (%) for C₈₇H₇₂F₂₄N₈O₂P₅ReRu: C, 48.38; H, 3.36; N, 5.19. Found: C, 48.40; H, 3.45; N, 5.06. ¹H-NMR (300 MHz, acetone-*d*₆) δ/ppm: 8.61 (s, 1H, β-bpy-3), 8.59 (s, 5H, α-bpy-3, dmb-3), 8.19 (s, 1H, γ-bpy-3), 8.16 (s, 1H, δ-bpy-3), 7.98 (d, *J* = 5.3 Hz, 1H, γ-bpy-6), 7.80–7.78 (m, 2H, β-bpy-6, α-bpy-6), 7.74–7.72 (m, 5H, δ-bpy-6, dmb-6), 7.38 (d, *J* = 6.0 Hz, 1H, β-bpy-5), 7.32–7.25 (m, 17H, α-bpy-5, dmb-5, Ph-*o*), 7.04 (dd, *J*_{HH} = 8.6 Hz, *J*_{FH} = 8.6 Hz, 12H, Ph-*m*), 6.96 (d, *J* = 5.6 Hz, 1H, γ-bpy-5), 6.90 (d, *J* = 5.9 Hz, 1H, δ-bpy-5), 2.86 (s, 2H, β-CH₂), 2.78 (s, 2H, γ-CH₂), 2.50–2.40 (m, 18H, dmb-CH₃, α-bpy-CH₃, δ-bpy-CH₃), 2.01 (tt, 4H, *J* = 2.1 Hz, 2.1 Hz, –CH₂–CH₂–CH₂–). FT-IR (in CH₂Cl₂) ν_{CO}/cm⁻¹: 1868, 1938. ESI-MS (eluent: MeCN) *m/z*: 575 ([M – 3PF₆⁻]³⁺), 935 ([M – 2PF₆⁻]²⁺).

Synthesis of [(dmb)₂Ru(CH₂OCH₂)Re(CO)₃Br](PF₆)₂ (Ru(CH₂OCH₂)Re(CO)₃Br). **Ru(CH₂OCH₂)** (68.5 mg, 0.06 mmol) and Re(CO)₅Br (32.5 mg, 0.08 mmol) were dissolved in EtOH (60

mL), and the solution was refluxed for 5 h under an N₂ atmosphere in the absence of light. After evaporation of the solvent, **Ru(CH₂OCH₂)Re(CO)₃Br** was isolated by ion-exchange column chromatography on a SP Sephadex C-25 column using acetonitrile–water (1 : 1 v/v) containing NH₄PF₆ as the eluent. Although a small amount of **Ru(CH₂OCH₂)Re(CO)₃(MeCN)** byproduct was present as a contaminant, the recovered sample was used in the subsequent synthesis without further purification. Yield: 66.5 mg (crude). FT-IR (in CH₂Cl₂) ν_{CO}/cm⁻¹: 2039, 2022, 1919. ESI-MS (eluent: MeCN) *m/z*: 600 ([M – 2PF₆⁻]²⁺).

Synthesis of [(dmb)₂Ru(CH₂OCH₂)Re(CO)₃(MeCN)](PF₆)₃·H₂O (Ru(CH₂OCH₂)Re(CO)₃(MeCN)). The crude sample (75.3 mg) of **Ru(CH₂OCH₂)Re(CO)₃Br** containing **Ru(CH₂OCH₂)Re(CO)₃(MeCN)** and CF₃SO₃H (0.03 mL, 0.34 mmol) were dissolved in *o*-dichlorobenzene (7 mL), and the solution was refluxed for 5 h under an Ar atmosphere in the absence of light. After evaporation of the solvent, the product was isolated by ion-exchange column chromatography on a CM Sephadex C-25 column using MeCN–H₂O (1 : 1 v/v) containing NH₄PF₆ as the eluent. After evaporation of the solvent, **Ru(CH₂OCH₂)Re(CO)₃(MeCN)** was obtained by recrystallization from a CH₂Cl₂–diethyl ether mixed solution as a red solid. The yield was 70% (56.5 mg, 0.05 mmol). Elemental analysis calcd (%) for C₅₃H₅₁F₁₈N₉O₅P₃ReRu: C, 39.39; H, 3.18; N, 7.80. Found: C, 39.36; H, 3.19; N, 7.71. ¹H-NMR (300 MHz, acetonitrile-*d*₃) δ/ppm: 8.96 (d, *J* = 5.9 Hz, 1H, β-bpy-6), 8.85 (d, *J* = 5.7 Hz, 1H, α-bpy-6), 8.47 (s, 1H, β-bpy-3), 8.44 (s, 1H, α-bpy-3), 8.37 (s, 1H, γ-bpy-3), 8.34 (s, 1H, δ-bpy-3), 8.32 (s, 4H, dmb-3), 7.70 (d, *J* = 5.7 Hz, 1H, γ-bpy-6), 7.68 (d, *J* = 6.2 Hz, 1H, β-bpy-5), 7.55–7.49 (m, 6H, δ-bpy-6, dmb-6, α-bpy-5), 7.39 (d, *J* = 5.7 Hz, 1H, γ-bpy-5), 7.21–7.20 (m, 5H, δ-bpy-5, dmb-5), 4.91 (s, 2H, β-CH₂), 4.88 (s, 2H, γ-CH₂), 2.56–2.51 (m, 18H, dmb-CH₃, β-bpy-CH₃, γ-bpy-CH₃), 2.04 (s, 3H, CH₃–CN⁻). FT-IR (in MeCN) ν_{CO}/cm⁻¹: 2039, 1934. ESI-MS (eluent: MeCN) *m/z*: 600 ([M – MeCN + Br⁻ – 3PF₆⁻]³⁺), 655 ([M – 2PF₆⁻]²⁺).

Synthesis of [(dmb)₂Ru(CH₂OCH₂)Re(CO)₃(OC(O)OC₂H₄N(C₂H₄OH)₂)](PF₆)₂ (Ru(CH₂OCH₂)Re(CO)₃(X)). **Ru(CH₂OCH₂)Re(CO)₃(MeCN)** was dissolved in DMF, and the resulting solution was stirred overnight. TEOA was added to the solution, and the solution was stirred for an hour to give a mixture of **Ru(CH₂OCH₂)Re(CO)₃(DMF)** and **Ru(CH₂OCH₂)Re(CO)₃(TEOA)**. **Ru(CH₂OCH₂)Re(CO)₃(X)** was obtained by bubbling the solution with CO₂ for 10 min. The reversibility of this CO₂ insertion reaction was confirmed by the recovery of the starting complexes in the solution after bubbling with Ar for 20 min. FT-IR (in MeCN) ν_{CO}/cm⁻¹: 2006, 2018 (Fig. S5, ESI[†]).

Conclusions

The greatest photocatalytic activity for CO₂ reduction using BNAH as the reductant was achieved using **Ru(CH₂OCH₂)Re** ($\Phi_{\text{CO}} = 0.18$, TON_{CO} = 253). Introduction of an oxygen atom into the bridging unit improved the oxidation power of the excited Ru unit in the diad and increased the driving force of the intramolecular electron transfer from the OER species of the Ru unit to the Re unit. During the photocatalytic reaction, a part of the used **Ru(CH₂OCH₂)Re** was converted into



Ru(CH₂OCH₂)Re(CO)₃(X) (X = ⁻OC₂H₄N(C₂H₄OH)₂ or ⁻OC(O)-OC₂H₄N(C₂H₄OH)₂) during the initial stage of the photocatalytic reaction. The 3 : 1 mixture of **Ru(CH₂OCH₂)Re** and **Ru(CH₂OCH₂)Re(CO)₃(X)**, which respectively functioned as a photosensitizer and a photocatalyst in the photostationary state, efficiently photocatalyzed CO₂ reduction for an extended period.

Acknowledgements

This work was partially supported by the All Nippon Artificial Photosynthesis Project for Living Earth (AnApple) of JSPS and the Photon and Quantum Basic Research Coordinated Development Program (MEXT).

Notes and references

- (a) H. Arakawa, M. Aresta, J. N. Armor, M. A. Barteau, E. J. Beckman, A. T. Bell, J. E. Bercaw, C. Creutz, E. Dinjus, D. A. Dixon, K. Domen, D. L. DuBois, J. Eckert, E. Fujita, D. H. Gibson, W. A. Goddard, D. W. Goodman, J. Keller, G. J. Kubas, H. H. Kung, J. E. Lyons, L. E. Manzer, T. J. Marks, K. Morokuma, K. M. Nicholas, R. Periana, L. Que, J. Rostrup-Nielsen, W. M. H. Sachtler, L. D. Schmidt, A. Sen, G. A. Somorjai, P. C. Stair, B. R. Stults and W. Tumas, *Chem. Rev.*, 2001, **101**, 953; (b) H. Inoue, T. Shimada, Y. Kou, Y. Nabetani, D. Masui, S. Takagi and H. Tachibana, *ChemSusChem*, 2011, **4**, 173.
- V. Balzani, A. Juris, M. Ventyri, S. Campagna and S. Serroni, *Chem. Rev.*, 1996, **96**, 759.
- (a) E. Fujita, *Coord. Chem. Rev.*, 1999, **185–186**, 373; (b) H. Takeda and O. Ishitani, *Coord. Chem. Rev.*, 2010, **254**, 346.
- (a) J. Hawecker, J.-M. Lehn and R. Ziessel, *J. Chem. Soc., Chem. Commun.*, 1983, 536; (b) R. Ziessel, J. Hawecker and J.-M. Lehn, *Helv. Chim. Acta*, 1986, **69**, 1065; (c) A. H. A. Tinnemans, T. P. M. Koster, D. H. M. W. Thewissen and A. Mackor, *Recl. Trav. Chim. Pays-Bas*, 1984, **103**, 288; (d) J. L. Grant, K. Goswami, L. O. Spreer, J. W. Otvos and M. Calvin, *J. Chem. Soc., Dalton Trans.*, 1987, 2105; (e) H. Ishida, T. Terada, K. Tanaka and T. Tanaka, *Inorg. Chem.*, 1990, **29**, 905.
- C. Costentin, M. Robert and J.-M. Savéant, *Chem. Soc. Rev.*, 2013, **42**, 2423.
- (a) Y. Yan, E. L. Zeitler, J. Gu, Y. Hu and A. B. Bocarsly, *J. Am. Chem. Soc.*, 2013, **135**, 14020; (b) E. B. Cole, P. S. Lakkaraju, D. M. Rampulla, A. J. Morris, E. Abelev and A. B. Bocarsly, *J. Am. Chem. Soc.*, 2010, **132**, 11539.
- (a) K. Kiyosawa, N. Shiraishi, T. Shimada, D. Masui, H. Tachibana, S. Takagi, O. Ishitani, D. A. Tryk and H. Inoue, *J. Phys. Chem. C*, 2009, **113**, 11667; (b) Y. Kou, S. Nakatani, G. Sunagawa, Y. Tachikawa, D. Masui, T. Shimada, S. Takagi, D. A. Tryk, Y. Nabetani, H. Tachibana and H. Inoue, *J. Catal.*, 2014, **310**, 57; (c) A. Gabrielsson, F. Hartl, H. Zhang, J. R. Lindsay Smith, M. Towrie, A. Vlček Jr and R. N. Perutz, *J. Am. Chem. Soc.*, 2006, **128**, 4253; (d) J. Schneider, K. Q. Vuong, J. A. Calladine, X.-Z. Sun, A. C. Whitwood, M. W. George and R. N. Perutz, *Inorg. Chem.*, 2011, **50**, 11877; (e) S. Sato, T. Arai, T. Morikawa, K. Uemura, T. M. Suzuki, H. Tanaka and T. Kajino, *J. Am. Chem. Soc.*, 2011, **133**, 15240.
- (a) B. Gholamkhash, H. Mametsuka, K. Koike, T. Tanabe, M. Furue and O. Ishitani, *Inorg. Chem.*, 2005, **44**, 2326; (b) Y. Tamaki, K. Koike, T. Morimoto and O. Ishitani, *J. Catal.*, 2013, **304**, 22; (c) K. Koike, S. Naito, S. Sato, Y. Tamaki and O. Ishitani, *J. Photochem. Photobiol., A*, 2009, **207**, 109; (d) S. Sato, K. Koike, H. Inoue and O. Ishitani, *Photochem. Photobiol. Sci.*, 2007, **6**, 454; (e) Y. Tamaki, K. Watanabe, K. Koike, H. Inoue, T. Morimoto and O. Ishitani, *Faraday Discuss.*, 2012, **155**, 115; (f) G. Sahara and O. Ishitani, *Inorg. Chem.*, DOI: 10.1021/ic502675a.
- K. Sekizawa, K. Maeda, K. Domen, K. Koike and O. Ishitani, *J. Am. Chem. Soc.*, 2013, **135**, 4596.
- (a) O. Ishitani, M. W. George, T. Ibusuki, F. P. A. Johnson, K. Koike, K. Nozaki, C. Pac, J. J. Turner and J. R. Westwell, *Inorg. Chem.*, 1994, **33**, 4712; (b) H. Tsubaki, A. Sekine, Y. Ohashi, K. Koike, H. Takeda and O. Ishitani, *J. Am. Chem. Soc.*, 2005, **127**, 15544; (c) H. Tsubaki, A. Sugawara, H. Takeda, B. Gholamkhash, K. Koike and O. Ishitani, *Res. Chem. Intermed.*, 2007, **33**, 37.
- T. Morimoto, T. Nakajima, S. Sawa, R. Nakanishi, D. Imori and O. Ishitani, *J. Am. Chem. Soc.*, 2013, **135**, 16825.
- H. Takeda, Y. Yamamoto, C. Nishiura and O. Ishitani, *Anal. Sci.*, 2006, **22**, 545.
- J. G. Calvert and J. N. Pitts, *Photochemistry*, Wiley and Sons, New York, 1966.
- D. Mauzerall and F. Westheimer, *J. Am. Chem. Soc.*, 1955, **77**, 2261.
- C. M. Elliott, D. L. Derr, S. Ferrere, M. D. Newton and Y.-P. Liu, *J. Am. Chem. Soc.*, 1996, **118**, 5221.
- S. Ferrere and C. M. Elliott, *Inorg. Chem.*, 1995, **34**, 5818.
- B. P. Sullivan, D. J. Salmon and T. J. Meyer, *Inorg. Chem.*, 1978, **17**, 3334.
- Y. Tamaki, K. Koike, T. Morimoto, Y. Yamazaki and O. Ishitani, *Inorg. Chem.*, 2013, **52**, 11902.

